Eur. Phys. J. A **9**, 371–383 (2000)

THE EUROPEAN PHYSICAL JOURNAL A

Prompt light particle emission in the ^{36}Ar + ^{58}Ni reaction at 95 MeV/nucleon

P. Pawłowski[1a], B. Borderie[1], G. Auger[2], Ch.O. Bacri[1], N. Bellaize[3], F. Bocage[3], R. Bougault[3], R. Brou[3], P. Buchet[4], J.L. Charvet[4], A. Chbihi[2], J. Colin[3], D. Cussol[3], R. Dayras[4], A. Demeyer[5], D. Doré[4], D. Durand[3], J.D. Frankland[2], E. Galichet[1,8], E. Genouin-Duhamel[3], E. Gerlic[5], D. Guinet[5], P. Lautesse[5], J.L. Laville[2], J.F. Lecolley[3], R. Legrain[4], N. Le Neindre[3], O. Lopez[3], M. Louvel[3], A.M. Maskay[5], L. Nalpas[4], A.D. Nguyen[3], M. Pârlog[6], J. Péter[3], E. Plagnol[1], M.F. Rivet[1], E. Rosato[7], F. Saint-Laurent[2,b], S. Salou[2], J.C. Steckmeyer[3], M. Stern[5], G. Tăbăcaru[6], B. Tamain[3], L. Tassan-Got[1], O. Tirel[2], E. Vient[3], C. Volant[4], and J.P. Wieleczko[2]
(INDRA Collaboration)

[1] Institut de Physique Nucléaire, IN2P3-CNRS, F-91406 Orsay Cedex, France
[2] GANIL, CEA and IN2P3-CNRS, B.P. 5027, F-14076 Caen Cedex, France
[3] LPC, IN2P3-CNRS, ISMRA and Université, F-14050 Caen Cedex, France
[4] DAPNIA/SPhN, CEA/Saclay, F-91191 Gif sur Yvette Cedex, France
[5] Institut de Physique Nucléaire, IN2P3-CNRS and Université, F-69622 Villeurbanne Cedex, France
[6] National Institute for Physics and Nuclear Engineering, RO-76900 Bucharest-Măgurele, Romania
[7] Dipartimento di Scienze Fisiche and Sezione INFN, Università di Napoli "Federico II", I-80126 Napoli, Italy
[8] Conservatoire National des Arts et Métiers, F-75141 Paris Cedex 03, France

Received: 27 July 2000 / Revised version: 23 October 2000
Communicated by P. Schuck

Abstract. The prompt component at intermediate velocity of light charged particles is investigated. An improved coalescence model coupled to the intra-nuclear cascade code ISABEL is used to obtain light complex particle energy spectra and multiplicities as a function of impact parameter. The results are compared with experimental data from the ^{36}Ar + ^{58}Ni experiment at 95 MeV/nucleon, performed with the INDRA 4π detection system. The calculated prompt component is found to rather well reproduce proton spectra. For complex light charged particles the calculated components well populate the high energy part of spectra. Prompt emission can therefore explain the large transverse energies experimentally observed at mid-rapidity.

PACS. 24.10.-i Nuclear-reaction models and methods – 25.70.Lm Strongly damped collisions – 25.70.Pq Multifragment emission and correlations

1 Introduction

A good understanding of the reaction mechanisms between heavy ions at intermediate energies is of major interest. Indeed, the dissipative collisions involved are a tool of choice to produce and investigate nuclei at large excitation energies and temperatures. The precise characterization of the hot nuclei produced calls for a detailed comprehension of the mechanisms since dynamical or out of equilibrium effects are known to play an important role in this energy regime. For energies below 10–15 MeV/nucleon dissipative collisions are dominated by mean-field effects giving rise to complete fusion or binary deep inelastic collisions (DIC) [1], whereas for much higher energies, above 200 MeV/nucleon, nucleon-nucleon (N-N) collisions take over and the reactions can be interpreted in a participant-spectator framework: here, two excited spectators are accompanied by a very hot fireball created in the interaction zone of the colliding nuclei. The situation in the intermediate energy domain is more complicated. This region exhibits a transitional regime where two-body collisions come into play and compete more and more with the mean field as the incident energy increases. The importance of two-body collisions is particularly revealed by some direct experimental facts such as pre-equilibrium emitted particles and high energy γ-rays [2–4]. But it also appears, in an indirect way, through dynamical properties of collisions showing deviations from the pure binary pictures (DIC) observed at lower incident energy [5–22]. Such deviations are predicted in the framework of transport theories: Boltzmann-Nordheim-Vlasov

[a] e-mail: pawlow@ipno.in2p3.fr
[b] *Present address*: DRFC/STEP, CEA/Cadarache, F-13018 Saint-Paul-lez-Durance Cedex, France

(BNV) [23], Boltzmann-Uehling-Uhlenbeck (BUU) [24], or Landau-Vlasov (LV) [25]. For heavy systems, depending on the incident energy and impact parameter, the formation of a neck between the two partners of a collision can be observed [12]. Different evolutions with time are possible: rupture from the two main outgoing nuclei, which constitutes a third emission source, or re-absorption by one of the two partners, which leads to the formation of very deformed nuclei and consequently to favored directed particle emission or fission [7,8,17]. For light systems an emission coming from the overlap zone between the two colliding nuclei is also predicted [19,26].

Thus, emissions of different types are predicted to populate the intermediate velocity region, that we can classify in two groups. One is related to "direct-pre-equilibrium-prompt" processes that we shall define to simplify as prompt emissions; the second is rather governed by reaction dynamics (neck-deformation). The aim of this paper is to bring information about the quantitative contribution from the first emission type. Prompt complex particle emission was recently calculated in BUU simulations, taking into account three-body correlations [27,28], and well compared to experimental data [29,30]. In another approach, Antisymmetrized Molecular Dynamics (AMD) calculations coupled to a coalescence process was found to reproduce experimental complex particle multiplicities at 150 MeV/nucleon [31]. In this paper we propose a new approach: a calculation which couples the intra-nuclear cascade code ISABEL (producing prompt protons and neutrons) to an improved version of coalescence model. For comparison, experimental light charged particle (LCP) spectra in the intermediate velocity region, obtained with the INDRA 4π detector on the ^{36}Ar + ^{58}Ni system at 95 MeV/nucleon have been selected and confronted to the model. Both multiplicities and energy spectra are compared.

In section 2 we describe the ISABEL code, and present a slightly extended version of the coalescence model. In section 3 the experimental details and results are presented. Section 4 contains comparison of LCP energy spectra and mean multiplicities and kinetic energies obtained in the simulation, with the corresponding experimental observables. We estimate also the excitation energy, remaining in the system after direct emission. Finally, conclusion of our investigation will be presented.

2 Calculation of the prompt component

2.1 The Intra-nuclear Cascade code ISABEL

This model, developed by Yariv and Fraenkel [32], treats colliding ions as two clouds of nucleons residing in potential wells. The projectile is Lorentz contracted in the target rest frame. The momentum distribution of nucleons in each of the collision partners is assumed to be that of a degenerated Fermi gas. In the overlap region a number of primary N-N collisions occurs, leading to a cascade of collisions in each of the reaction partners. N-N scattering is described by experimentally measured free N-N cross-sections. The Pauli blocking is assured by the interdiction for cascade particle energy to fall below the Fermi energy. Interaction between two particles from the same Fermi sea is also forbidden.

Each cascade particle is followed until it leaves the overlap region. Outside of this region the particle is followed until it leaves the system, or until its energy falls below a given cut-off energy. In the latter case, it is captured by one of the nuclei and its energy contributes to the excitation energy of the main outgoing partners. The cut-off energy is a free parameter of the model and is taken from the prescription proposed in ref. [33]:

$$E_{\rm cut} = \begin{cases} E_{\rm F} + \max(2B, V_{\rm C}), & \text{for protons,} \\ E_{\rm F} + 2B, & \text{for neutrons,} \end{cases} \quad (1)$$

where $E_{\rm F}$ is the Fermi energy, B is the average binding energy (calculated for three first neutrons and protons), and $V_{\rm C}$ is the Coulomb barrier.

The nuclear density distributions in both the projectile and the target are approximated by a step-function distribution. As a cascade develops, the density in the participating Fermi seas is depleted. After each collision a hole is punched in the density distribution. No more interactions are allowed in this site (so-called "slow rearrangement"). Excitation energies of the two outgoing nuclei are the sums of the hole energies and of the energies of the captured particles which fall below the cut-off energy.

The model was first developed for experiments in the relativistic energy domain, where N-N interactions dominate. In our application at rather low energy we expect the model to work properly for mid-central and peripheral collisions. Because mean-field effects are neglected (one-body collisions), energy dissipation is never correctly estimated. This prevents any precise information on excitation energies at all impact parameters. Moreover, the fixed density approximation made in the calculation is especially unrealistic for central collisions. Consequently, we shall not use excitation energy from the code to simulate the de-excitation component. As a lower limit of applicability of the model we have taken an impact parameter $b = 4$ fm which corresponds to about $0.42 b_{\rm max}$. Such a limit is suggested by [22]: in this range of impact parameters the total mass of particles emitted at mid-velocity was found equal to that contained in the overlap zone between projectile and target, at least if one assumes independence of mid-rapidity emission of incident energy.

In fig. 1 we present the average multiplicities of protons and neutrons leaving the system as a function of impact parameter for ^{36}Ar + ^{58}Ni reactions at incident energy 95 MeV/nucleon. The number of neutrons is approximately equal to that of protons, with a small deviation corresponding to the neutron-to-proton ratio in the reaction, which is equal to 1.04. Energy spectra are also similar for neutrons and protons. In fig. 2 direct nucleons in momentum space are presented in the form of $E{\rm d}^2\sigma/p_\perp {\rm d}p_\perp {\rm d}p_\parallel$ Lorentz invariant differential cross-sections.

Characteristic circles around projectile and target momenta correspond to the cut-off energy parameters. Below

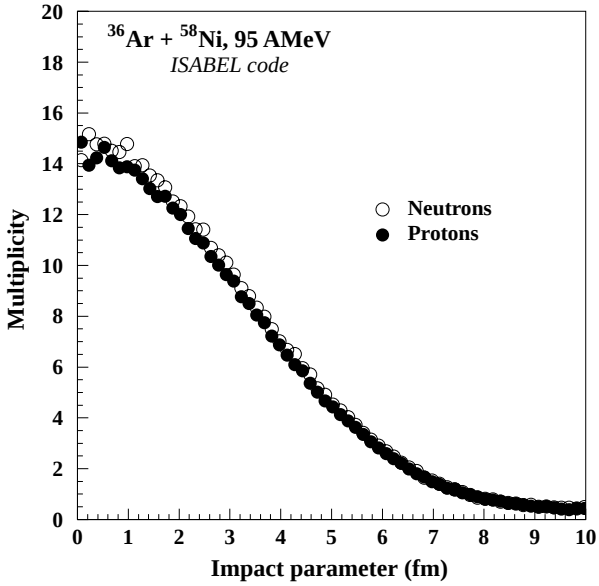

Fig. 1. ISABEL simulation results. Average multiplicities of direct nucleons as a function of impact parameter, at the end of the cascade step.

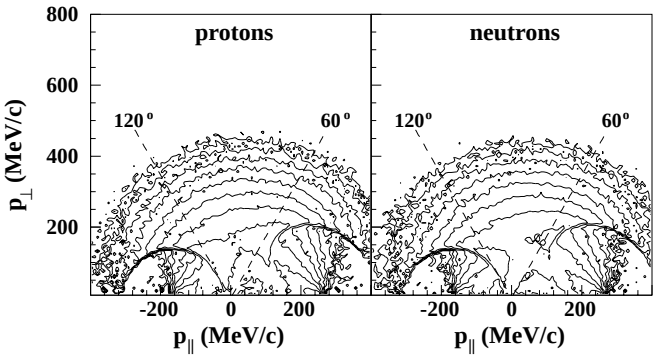

Fig. 2. ISABEL simulation results. Lorentz invariant differential cross-sections for direct protons and neutrons in momentum space (c.m. reference frame), integrated over the whole impact parameter range. Statistics between two neighboring contour lines changes by a factor of 2.

this limit one can observe a number of nucleons escaping directly from the overlap region (the cut-off energy test is not performed for these particles). Some deformation of the cut-off energy circle around the projectile is due to problems with transfer of projectile potential energy to the target rest frame in a covariant way [34].

To perform a careful study of LCP emission in the intermediate velocity region we have restricted our analysis to particles with polar angles between 60° and 120° in the center of mass (marked by dashed lines in fig. 2).

2.2 Coalescence model

2.2.1 Standard form

The coalescence model, proposed by Butler and Pearson in 1963 [35] was successfully used in describing LCP energy spectra in heavy-ion experiments at relativistic energies [36–41]. The first suggestion, that observed deuteron densities in momentum space can be described as proportional to the product of proton and neutron densities, was extended by Schwarzschild and Zupančič for the case of more complex particles, like tritons, ^{3}He, and ^{4}He [42]. A formal correspondence between the coalescence model and a thermodynamic calculation for equilibrated fireball was also shown by Mekjian [43].

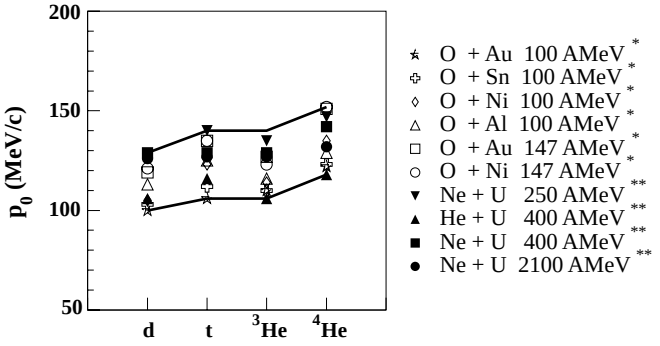

Fig. 3. p_0 values experimentally measured. Results marked by * (**) are taken from ref. [40] ([36]). The solid lines indicate the limits taken in present paper.

In principle, the model treats light complex particles as clusters of emitted nucleons, formed in a reaction. This process is expected to take place in the vicinity of or even inside the colliding ions, because an interaction of joined nucleons with a nuclear potential is necessary for energy conservation [35]. It is assumed that once formed, a complex particle does not decay, so the momentum vectors of joined nucleons should be reasonably close to each other. In the standard version of the model one assumes that a cluster composed of A nucleons is created at the point $\overrightarrow{p}_c$ in momentum (per nucleon) space, if all these nucleons occupy a "small" sphere of radius p_0, centered at $\overrightarrow{p}_c$ [36,44]. The radius p_0 is the only free parameter of the model and can be determined by simple fit to experimental data. The p_0 parameters, relative to the different complex particles, are expected to be independent of incident energy and colliding systems. Within error bars this is rather well observed over a broad incident energy range from around 100 MeV/nucleon to 100 GeV/nucleon [41]. Figure 3 presents p_0 parameters for d, t, ^{3}He, and ^{4}He particles, obtained in refs. [36,40] in our incident energy region.

We can see that p_0 values vary from about 100 MeV/c to about 150 MeV/c depending on complex particle. As can be checked in fig. 2, the diameter $2p_0$ of our sphere cannot be treated as negligible in comparison with the available volume in momentum space. Direct nucleon density can change strongly inside the sphere and cannot be approximated by a constant value, given by the density in the center of the sphere. So, calculations presented in [44] correspond to some approximation, justified for high incident energies when the momentum space is also sufficiently large, but not at lower energies. In this latter case, the average number of particles occupying the sphere can

no longer be expressed by the simple product of the volume $\frac{4}{3}\pi p_0^3$ by the nucleon density at the center of the sphere, but should rather be calculated as an integral of density over the whole sphere.

Usually, the coalescence model is applied starting from experimental proton spectra (neutron spectra are supposed to be identical to proton ones, corrected for N/Z of the studied system). Then, complex particle spectra are built using the formula

$$\frac{\mathrm{d}^3\sigma_{ZN}}{\mathrm{d}p^3} = \left(\frac{N_\mathrm{T}+N_\mathrm{P}}{Z_\mathrm{T}+Z_\mathrm{P}}\right)^N \frac{1}{N!Z!}\left(\frac{4\pi p_0^3}{3\sigma_0}\right)^{A-1}\left(\frac{\mathrm{d}^3\sigma_\mathrm{P}}{\mathrm{d}p^3}\right)^A, \tag{2}$$

where $\frac{\mathrm{d}^3\sigma_{ZN}}{\mathrm{d}p^3}$ is the differential cross-section of a cluster composed of Z protons and N neutrons, $\frac{\mathrm{d}^3\sigma_\mathrm{P}}{\mathrm{d}p^3}$ is the differential cross-section for observed protons, N_T, N_P, Z_T, Z_P are neutron and proton numbers in target and projectile, $A = N + Z$ is the mass number of the cluster, and σ_0 the total reaction cross-section. In our case we dispose with ISABEL of complete information relative to "primary" protons and neutrons needed to produce complex particles. In such a way a more precise calculation can be envisaged.

2.2.2 Improved version

Let us consider the momentum (per nucleon) space of direct particles, emitted in a collision. We assume that direct nucleons are statistically independent, or, in other words, no N-N correlations occur. At the beginning we take into account a set of events with fixed direct particle multiplicity m. For each point $\overrightarrow{p}$ in momentum space one can determine direct particle density $\rho_m(\overrightarrow{p})$. Of course, an integration of $\rho_m(\overrightarrow{p})$ over the whole space gives the total multiplicity of direct particles m:

$$\int \rho_m(\overrightarrow{p})\,\mathrm{d}p^3 = m. \tag{3}$$

Now, let us take a point in momentum space, denoted by $\overrightarrow{p}_\mathrm{c}$, where a complex particle is created by clusterization of neighboring direct nucleons. For each point $\overrightarrow{p}$ we can determine a probability $P(\overrightarrow{p}, \overrightarrow{p}_\mathrm{c})$, that a nucleon placed in the point $\overrightarrow{p}$ will be used to form a complex particle in the point $\overrightarrow{p}_\mathrm{c}$. Now, one can determine the density of particles used for clusterization:

$$\widetilde{\rho}_m(\overrightarrow{p}, \overrightarrow{p}_\mathrm{c}) = \rho_m(\overrightarrow{p})\,P(\overrightarrow{p}, \overrightarrow{p}_\mathrm{c}). \tag{4}$$

In fact, $P(\overrightarrow{p}, \overrightarrow{p}_\mathrm{c})$ should be a function of the distance between $\overrightarrow{p}$ and $\overrightarrow{p}_\mathrm{c}$, $|\overrightarrow{p} - \overrightarrow{p}_\mathrm{c}|$, so an integration of $P(\overrightarrow{p}, \overrightarrow{p}_\mathrm{c})$ over the whole space gives a characteristic volume V (in momentum space), independent of the point $\overrightarrow{p}_\mathrm{c}$:

$$\int P(\overrightarrow{p}, \overrightarrow{p}_\mathrm{c})\,\mathrm{d}p^3 = \int P(\overrightarrow{p}, \overrightarrow{p}_\mathrm{c})\,\mathrm{d}p_\mathrm{c}^3 = V. \tag{5}$$

Dividing $P(\overrightarrow{p}, \overrightarrow{p}_\mathrm{c})$ by the volume V one obtains a corresponding density of probability λ, normalized to unity:

$$\lambda(\overrightarrow{p}, \overrightarrow{p}_\mathrm{c}) = \frac{1}{V}P(\overrightarrow{p}, \overrightarrow{p}_\mathrm{c}). \tag{6}$$

Now, using equations (3), (4) and (6), we calculate the probability of a nucleon to join a cluster located at the point $\overrightarrow{p}_\mathrm{c}$:

$$\begin{aligned} P_m(\overrightarrow{p}_c) &= \frac{\int \widetilde{\rho}_m(\overrightarrow{p})\,\mathrm{d}p^3}{\int \rho_m(\overrightarrow{p})\,\mathrm{d}p^3} = \frac{1}{m}\int \rho_m(\overrightarrow{p})\,P(\overrightarrow{p}, \overrightarrow{p}_c)\,\mathrm{d}p^3 \\ &= \frac{V}{m}\int \rho_m(\overrightarrow{p})\,\lambda(\overrightarrow{p}, \overrightarrow{p}_c)\,\mathrm{d}p^3. \end{aligned} \tag{7}$$

The last integral in (7) is a simple average value of nucleon density $\rho_m(\overrightarrow{p})$, weighted by $\lambda(\overrightarrow{p}, \overrightarrow{p}_\mathrm{c})$. The standard form in the model corresponds to the function λ with the prescription:

$$\lambda(\overrightarrow{p}, \overrightarrow{p}_\mathrm{c}) = \begin{cases} \frac{1}{V}, \text{ if } |\overrightarrow{p} - \overrightarrow{p}_\mathrm{c}| \le p_0 \\ 0, \text{ if } |\overrightarrow{p} - \overrightarrow{p}_\mathrm{c}| > p_0 \end{cases}, \tag{8}$$

where p_0 is the radius of the coalescence sphere, and $V = \frac{4}{3}\pi p_0^3$ is its volume. Such a choice is convenient because in this case both V and λ are characterized by the same parameter p_0. We keep this choice in the present work, but it should be stressed here that, in principle, V and λ can be considered as two independent quantities. Now, we can introduce (8) into (7) to obtain a simple formula for the probability P_m:

$$P_m(\overrightarrow{p}_\mathrm{c}) = \frac{1}{m}\int_V \rho_m(\overrightarrow{p})\,\mathrm{d}p^3. \tag{9}$$

In what follows, we use a reasoning similar to that presented in [44]. We calculate the conditional probability $P_{n/m}(\overrightarrow{p}_\mathrm{c})$ of clusterization of n nucleons in the point $\overrightarrow{p}_\mathrm{c}$, if m direct nucleons were emitted in the collision:

$$P_{n/m}(\overrightarrow{p}_\mathrm{c}) = \binom{m}{n} P_m^n\,(1-P_m)^{m-n}. \tag{10}$$

Then, the total probability of occurrence of a cluster composed of n nucleons is

$$P_n(\overrightarrow{p}_\mathrm{c}) = \sum_{m\ge n} f(m)\,P_{n/m}(\overrightarrow{p}_\mathrm{c}), \tag{11}$$

where $f(m)$ is the nucleon multiplicity distribution, normalized to unity. In fact, we have to distinguish neutron and proton densities and multiplicities. So, the probability $P_{ZN}(\overrightarrow{p}_\mathrm{c})$ of occurrence of a cluster consisting of Z protons and N neutrons is given by

$$P_{ZN}(\overrightarrow{p}_\mathrm{c}) = P_Z(\overrightarrow{p}_\mathrm{c})\,P_N(\overrightarrow{p}_\mathrm{c}), \tag{12}$$

where $P_Z(\overrightarrow{p}_\mathrm{c})$ and $P_N(\overrightarrow{p}_\mathrm{c})$ are given by eq. (11).

Our goal is to find density of complex particles in momentum space. Formula (12) gives the probability to form a cluster (Z, N) in the point $\overrightarrow{p}_\mathrm{c}$, if there exists in $\overrightarrow{p}_\mathrm{c}$ *a*

center of condensation. So, the complex particle density is given by

$$\rho_{ZN}\left(\overrightarrow{p}_{\mathrm{c}}\right) = \rho_c\left(\overrightarrow{p}_{\mathrm{c}}\right) P_{ZN}\left(\overrightarrow{p}_{\mathrm{c}}\right), \tag{13}$$

where $\rho_c\left(\overrightarrow{p}_{\mathrm{c}}\right)$ denotes the density of condensation centers in momentum space. The presence of the variable $\rho_c\left(\overrightarrow{p}_{\mathrm{c}}\right)$ is necessary to assure particle number conservation. Actually, the concept of condensation center is not so easy to define. If few nucleons attempt to form a cluster, they have to be sufficiently close to each other in configuration space, to interact by nuclear forces. One could say that if such a chance occurs, the sum of their momentum vectors divided by the nucleon number gives directly the point $\overrightarrow{p}_{\mathrm{c}}$ in our calculation. But, as the presence of a nuclear potential seems to be necessary to form a complex particle, the location of the point $\overrightarrow{p}_{\mathrm{c}}$ can be different. Moreover, in terms of the coalescence model, protons and neutrons observed as free particles are treated as one-nucleon clusters. These facts complicate strongly the sense of $\rho_c\left(\overrightarrow{p}_{\mathrm{c}}\right)$. As we do not know anything about conditions of cluster formation, we assume that condensation centers are distributed uniformly. Such an assumption is also taken implicitly in the standard version of the model.

If the condensation center density $\rho_c\left(\overrightarrow{p}_{\mathrm{c}}\right)$ is really uniform, it can be written in the form

$$\rho_c\left(\overrightarrow{p}_{\mathrm{c}}\right) = \frac{1}{\alpha V}, \tag{14}$$

where α is a constant. Inserting eq. (14) into eq. (13) one obtains the final formula for complex particle density:

$$\rho_{ZN}\left(\overrightarrow{p}_{\mathrm{c}}\right) = \frac{1}{\alpha V} P_{ZN}\left(\overrightarrow{p}_{\mathrm{c}}\right). \tag{15}$$

The constant α is not a free parameter of the model, because it is determined by nucleon number conservation. If one assumes that only p, d, t,^{3}He, and ^{4}He particles are formed in the model, the proton number conservation requires:

$$M'_{\mathrm{p}} = M_{\mathrm{p}} + M_{\mathrm{d}} + M_{\mathrm{t}} + 2M_{^3\mathrm{He}} + 2M_{^4\mathrm{He}}, \tag{16}$$

where M'_{p} is the number of primary protons, M_{p} is the number of secondary (not clusterized) protons, and M_{d}, M_{t}, $M_{^3\mathrm{He}}$, and $M_{^4\mathrm{He}}$ are the numbers of deuteron, triton, helium-3 and helium-4 particles, respectively. Secondary protons can be obtained from the model, taking $p_0 \to 0$. Variables on the right-hand side of eq. (16) depend on α. For a given density of primary protons and given p_0 parameters for d, t,^{3}He, and ^{4}He one can obtain a unique value of α satisfying this equation. But, as the density of protons is a function of collision centrality (see fig. 1), one can expect an evolution of α with impact parameter. In our calculation the α parameter varies from 1.08 to about 1.30, when the impact parameter decreases from 8 to 4 fm. Note that the α parameter is the scaling factor between primary and secondary proton spectra $\left(\alpha = M'_{\mathrm{p}}/M_{\mathrm{p}}\right)$.

To summarize, we can say that complex particle density is governed by

- Volume V, chosen as the volume of a sphere of radius p_0; this parameter changes the total cross-section for complex particle production, but does not change the shape of energy spectra.
- Function λ, taken in the form given by (8), so governed by the same parameter p_0.
- Proton and neutron densities ρ_m.
- Primary nucleon multiplicity distributions, separately for protons $\left(M'_{\mathrm{p}}\right)$ and for neutrons $\left(M'_{\mathrm{n}}\right)$.

In our calculation we take all the quantities we need, *i.e.* proton and neutron densities, and proton and neutron multiplicity distributions, directly from the intra-nuclear cascade model. Thus we built the average densities $\frac{1}{p^2}\frac{\mathrm{d}M'_{\mathrm{p}}}{\mathrm{d}p}$ and $\frac{1}{p^2}\frac{\mathrm{d}M'_{\mathrm{n}}}{\mathrm{d}p}$ as a function of $|\overrightarrow{p}|$, in the angular range considered (see fig. 2). These quantities are also used when part of the coalescence sphere extends beyond the considered region, *i.e.* when the sphere is centered close to the c.m. point or close to the region borders. To obtain complex particle density we use formula (15), *i.e.* we do not use any of the simplifications listed in appendix. Only p_0 is taken from previous experiments using formula (2). To take into account dispersion observed for p_0 values, our calculation has been performed with two sets of values indicated by solid lines in fig. 3.

2.3 Calculation consistency

The standard coalescence formula (2) treats complex particle production as a perturbation. Consequently, the primary proton spectra are same as the secondary ones. In our more precise calculation the primary proton spectra differ from secondary ones by the constant factor α. Nevertheless, we use experimental values of p_0 determined with the help of formula (2). In this situation we have to verify the correctness of such a procedure. Firstly we use alternatively two possible treatments of data: a) we use formula (15), applied to *primary* proton and neutron densities taken from ISABEL and b) as above, but without integration of density inside the sphere (*i.e.* we take into account the simplification no. 1 — see appendix).

Using these two treatments one obtains similar secondary proton spectra but different spectra for complex particles d, t, ^{3}He, and ^{4}He. We present them in fig. 4 for deuteron and alpha-particles as solid (a) and dashed (b) lines. Then we apply the formula (A.3) from appendix for the secondary protons obtained in (a) (dotted line in fig. 4). In this way we "simulate" a real situation of measurement of p_0. In all cases we keep the same values of p_0, corresponding to the lower limit presented in fig. 3.

One observes that dotted and dashed lines nearly coincide. A larger difference can be observed in the case of more central collisions, but slopes of both distributions are perfectly the same. This good agreement shows that one can use the same p_0 parameter when applying coalescence to primary or secondary proton spectra (remind that p_0 values are deduced from only the high-energy part of the spectra). The complete method (a) with integration of nucleon density over the sphere gives slightly broader spectra

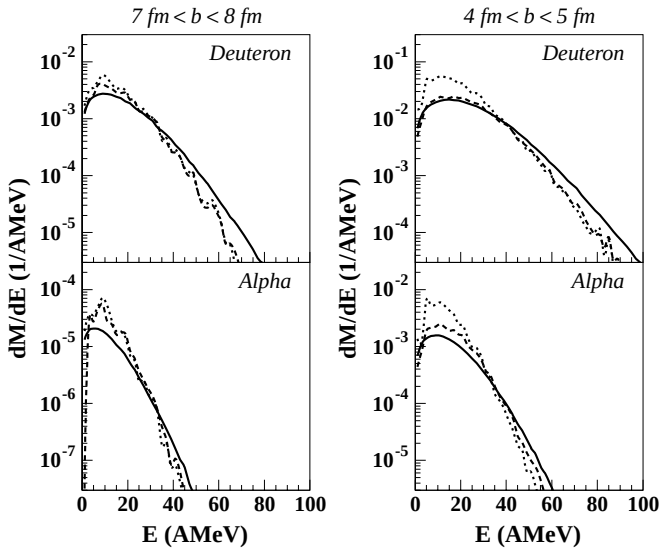

Fig. 4. Simulation results. Energy distributions for deuterons and alphas in two ranges of impact parameter. For solid, dashed and dotted lines see text.

and lower maxima. But this difference is just caused by a more correct calculation as compared to the previous cases and disappears at larger incident energies.

3 The experiment

3.1 Experimental set-up

The experiment was performed at the GANIL facility, using the INDRA 4π multi-detector system [45]. The ^{36}Ar beam was scattered on a ^{58}Ni target of 193 μg/cm^2 thickness. At least four detectors were required to fire as on-line trigger. The detection system contained a total number of 336 detection modules grouped in 17 rings. In the first ring covering the most forward angles, $2^\circ \leq \theta_{\rm LAB} \leq 3^\circ$, phoswich detectors were used, made of plastic scintillators NE102 + NE115. Between 3° and 45°, in eight rings, triple telescopes were employed, consisting of ionization chamber, silicon, and CsI(Tl) scintillator. Three rings between 45° and 88° contained double telescopes (ionization chamber + CsI(Tl)). In the five remaining rings, between 92° and 176°, CsI(Tl) detectors were installed. The total solid angle covered by detectors was about 90% of 4π. Light particle isotopes are separated up to $Z = 4$ in CsI(Tl) crystals. Charge identification reaches $Z = 64$ in the forward region (below 45°) and $Z = 20$ between 45° and 88°. In the absence of ionization chambers in the backward region (beyond 92°), separation of charges larger than 4 was there impossible. The LCP energy accuracy is equal to about 5% [46].

In our analysis we take into account the events where the total multiplicity of detected particles is larger than 3, and the total detected charge larger than or equal to 18 (*i.e.* argon charge). Other results of analysis of this experiment can be found in refs. [20,22,47–49].

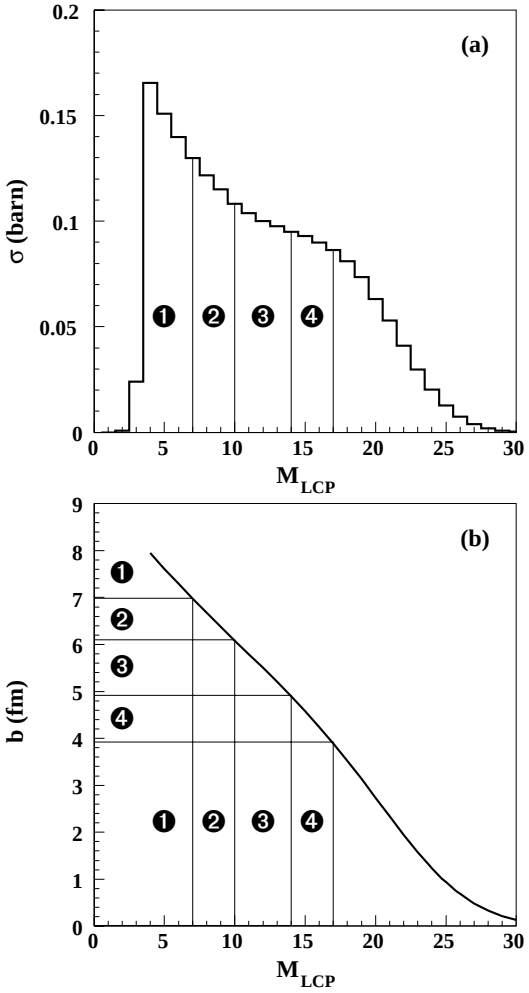

Fig. 5. Experimental LCP multiplicity distribution (a) and correspondence with impact parameter (b). Numbers 1 through 4 denote the four regions considered in the analysis.

3.2 Impact parameter selector

The impact parameter selector should be independent of studied observables, to avoid auto-correlation effects. In our investigation we would like to study the evolution of energy spectra with impact parameter. Therefore, one should avoid dynamic observables, like the transverse energy, isotropy ratio, or flow angle [50–53], because they influence directly the energy spectra. More useful are variables taking advantage of charge partition only, with no dynamic admixture. In this class the simplest one, multiplicity of LCP's ($Z \leq 2$), $M_{\rm LCP}$, is a good compromise: some auto-correlation effect can also occur in this case, because direct particles contribute to $M_{\rm LCP}$, nevertheless, it does not influence the shape of particle energy spectra.

In fig. 5 we present the experimental distribution of $M_{\rm LCP}$ (a) and a correspondence between $M_{\rm LCP}$ and impact parameter (b), obtained with the use of the geometrical prescription [54] and with a calculated $b_{\rm max}$ of 9.5 fm. Four regions were selected, marked from 1 to 4, each corresponding to about 1 fm range in impact parameter, be-

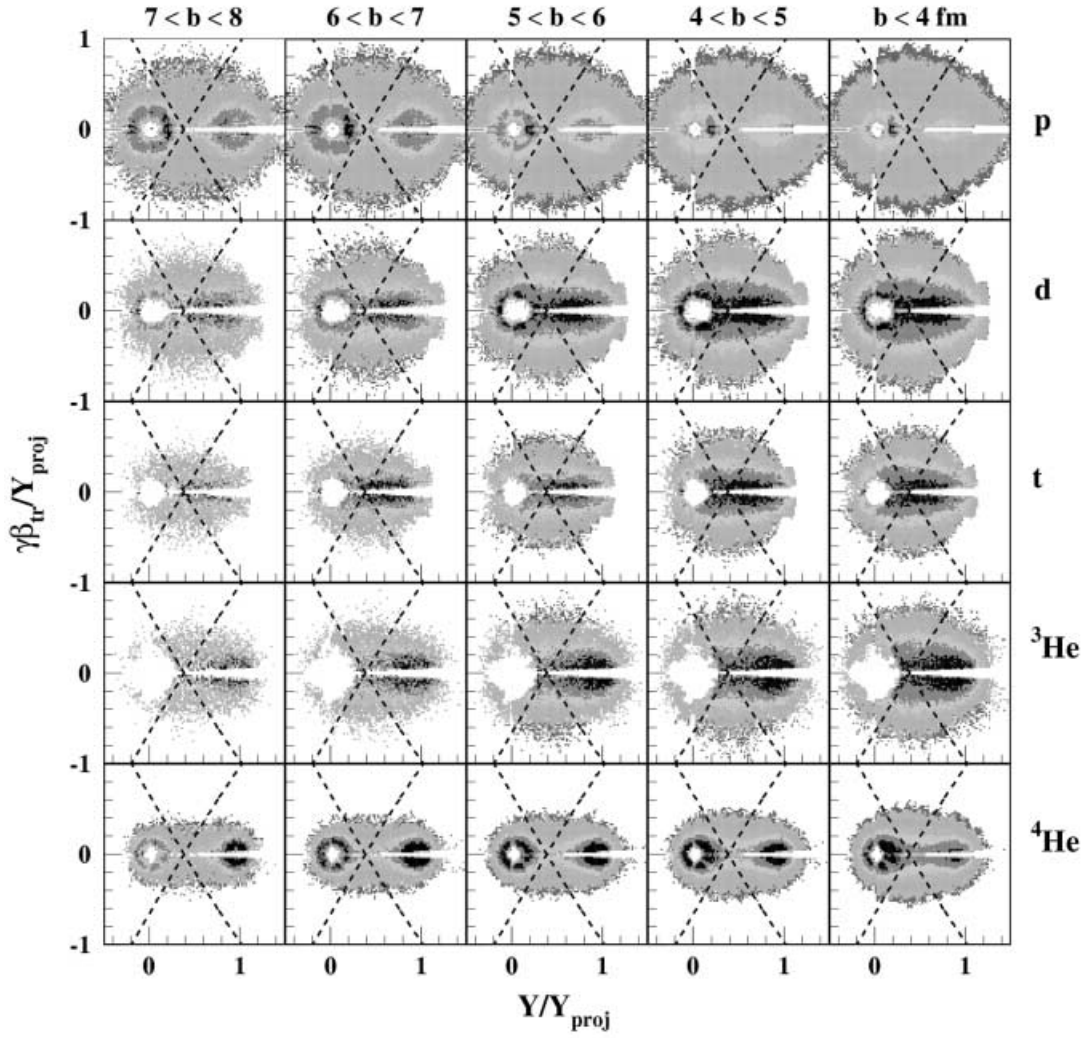

Fig. 6. Experimental data for ^{36}Ar + ^{58}Ni at 95 MeV/nucleon. Lorentz invariant cross-sections in $\gamma\beta_{\rm tr}$ *versus* rapidity plane for different LCPs and different "experimental" impact parameter ranges. The scales are expressed in units of the projectile rapidity $Y_{\rm proj}$. The dashed lines correspond to the c.m. angular range shown in fig. 2. The Z-axis is logarithmic.

tween 4 and 8 fm. This selection will be used in the following analysis. The experimental distribution of $Z_{\rm max}$ from QP was also used as impact parameter selector to avoid any possible auto-correlations. The LCP energy spectra as a function of the corresponding calculated impact parameter are found quasi-identical to those derived with the $M_{\rm LCP}$ selector.

3.3 Binary character of reactions

The binary character of the studied collisions appears in fig. 6. Invariant cross-section plots for different "experimental impact parameters" calculated with the use of $M_{\rm LCP}$ are presented in $\gamma\beta_{\rm tr}$ *versus* rapidity plane. One can clearly see characteristic circles around the projectile and the target momenta, especially in the case of protons and alphas, due to emission components from QP and QT. However, the figure also evidences the presence of a contribution at intermediate rapidities, around the c.m. rapidity and the N-N rapidity. As can be checked in [22], the increase of transverse energy in the intermediate rapidity region is observed around the N-N reference frame for protons, and rather around the c.m. for more complex particles. Both reference frames can be considered for observation of intermediate velocity emission. In the present paper we use c.m. reference frame for all particles. It should be mentioned here that switching to the N-N (or mid-rapidity) reference frame does not change the results. In fact, these two possible reference frames are fairly close to each other in our reaction.

The dashed lines correspond to the two limits for c.m. polar angle, imposed on simulation data (see fig. 2). In the selected mid-rapidity region evaporation components from QP and QT only contribute to small momenta, at least in the case of complex particles. For deuterons, tritons and helium-3 we observe a characteristic picture indicating a relatively important production of these particles at mid-rapidity [22].

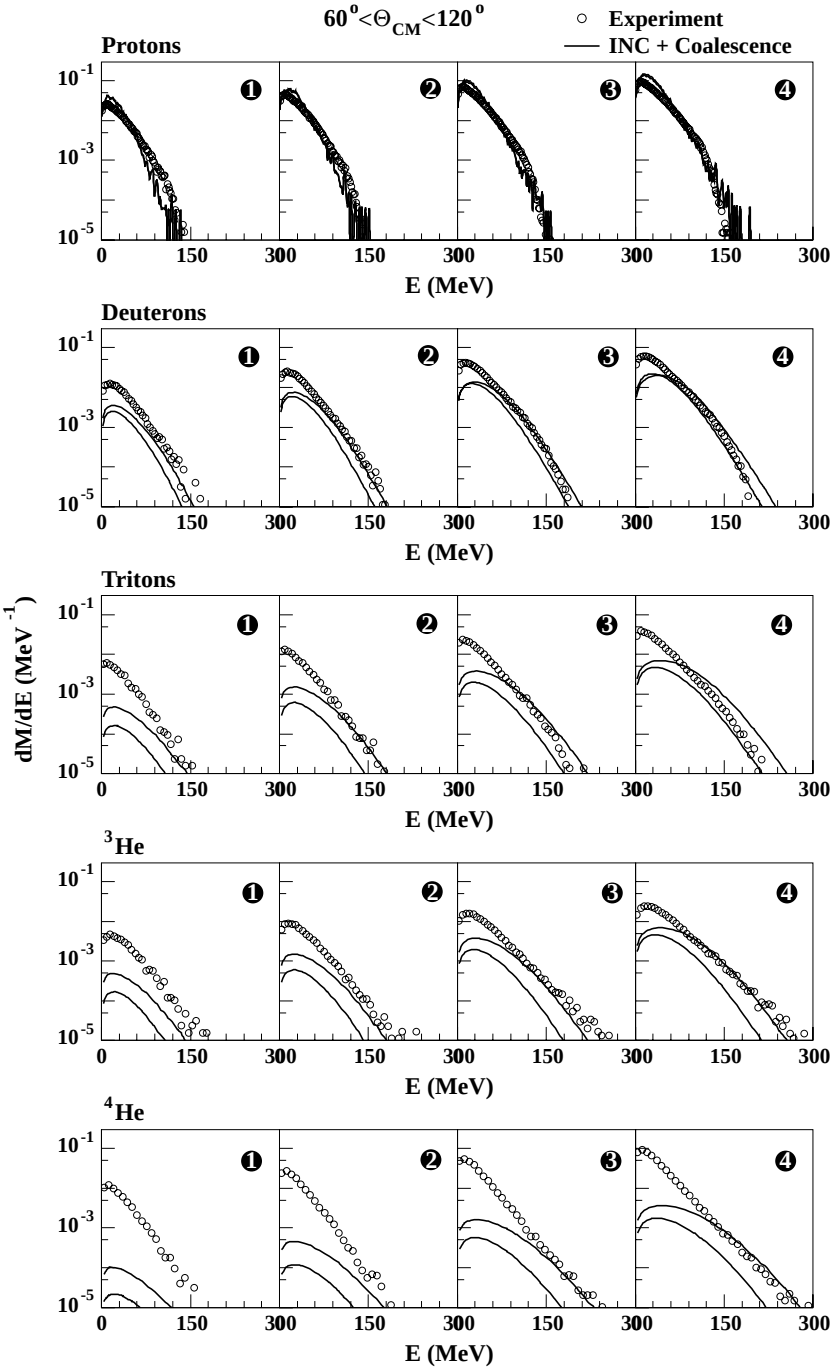

Fig. 7. LCP differential multiplicities dM/dE. Comparison of simulated energy spectra for p, d, t, ^{3}He, and ^{4}He (double solid lines) with experimental ones (circles). Impact parameter windows, marked from 1 to 4 are defined in fig. 5.

As excitation energies of QP and QT are not well predicted by the ISABEL code, we did not attempt to reproduce this de-excitation component in simulation, using some additional statistical code. We prefer to study only the prompt component, keeping in mind that a large contamination of prompt particles by thermal emission from the two main partners can be expected at small energies.

4 Comparison data-calculation

To obtain quantitative information on the contribution of prompt processes, we shall now compare energy spectra, multiplicities and mean kinetic energies obtained experimentally with those from the calculation previously described. There is no normalization between calculations and experimental spectra.

Table 1. Mean multiplicities and energies per nucleon of LCP's obtained in calculation as compared with experimental data. Calculated errors correspond to the two extreme hypotheses for p_0 values (see fig. 3).

b (fm)	Particle	$\overline{M}^{\rm exp}_{\rm tot}$	$\overline{M}^{\rm exp}_{60°\text{-}120°}$	$\overline{M}^{\rm calc}_{60°\text{-}120°}$		$\overline{E}^{\rm exp}_{60°\text{-}120°}$ (MeV/nucleon)	$\overline{E}^{\rm calc}_{60°\text{-}120°}$ (MeV/nucleon)	
7-8	p	3.41	0.49	0.66	± 0.02	26.5	23.4	
	d	0.54	0.142	0.041	± 0.009	15.3	17.8	± 0.8
	t	0.17	0.041	0.003	± 0.002	9.2	13.5	± 0.6
	^{3}He	0.17	0.038	0.003	± 0.002	11.4	13.3	± 0.6
	^{4}He	1.22	0.061	0.0005	± 0.0003	7.0	10.9	± 0.4
6-7	p	4.75	0.89	1.13	± 0.04	27.1	25.7	
	d	1.06	0.291	0.099	± 0.018	15.9	19.6	± 1.1
	t	0.35	0.090	0.012	± 0.006	9.8	15.1	± 0.8
	^{3}He	0.32	0.077	0.012	± 0.006	12.0	15.0	± 0.8
	^{4}He	2.13	0.135	0.0028	± 0.0017	7.0	12.4	± 0.6
5-6	p	5.83	1.43	1.89	± 0.08	28.7	27.4	
	d	1.74	0.521	0.216	± 0.025	17.1	22.1	± 1.6
	t	0.64	0.179	0.038	± 0.015	10.7	17.0	± 1.3
	^{3}He	0.56	0.151	0.037	± 0.014	13.4	16.9	± 1.3
	^{4}He	3.35	0.289	0.0122	± 0.0065	7.4	14.2	± 1.0
4-5	p	6.81	2.00	2.94	± 0.13	30.2	29.6	
	d	2.47	0.814	0.391	± 0.018	18.2	25.2	± 2.3
	t	1.00	0.308	0.088	± 0.026	11.6	19.7	± 1.9
	^{3}He	0.83	0.251	0.086	± 0.026	14.7	19.6	± 1.9
	^{4}He	4.31	0.512	0.0351	± 0.0154	8.0	16.7	± 1.6

4.1 LCP energy spectra

In calculations we use the complete formula given by eq. (15). Figure 7 presents energy distributions for p, d, t, ^{3}He, and ^{4}He in four impact parameter windows, defined in fig. 5. Impact parameter decreases from the left to the right. Double solid lines correspond to the two limits for p_0, indicated in fig. 3. For deuterons, which are the most produced coalescence particles, a good agreement can be observed, except in the region of smaller energies, where a contribution of evaporative components from QP and QT is expected. Increasing the mass of complex particles, contributions from prompt emissions decrease and only populate correctly the high tails of energy spectra. These results clearly reveal the importance of prompt processes for populating the high-energy parts of complex particle spectra.

The proton spectra are not so well reproduced, because of an excess of protons in the lower energy region and slopes somewhat too steep at large impact parameter. This last effect reflects in the small disagreement, observed at large energies, for complex particles in impact parameter regions 1 and 2, as compared to experimental data. However, without any normalization the agreement is remarkable and we can infer, as expected, that the major part of protons in the selected region comes from prompt processes.

4.2 LCP characteristics

In table 1 we summarize characteristic parameters obtained from energy spectra presented in fig. 7. Integrating over energy we obtained mean particle multiplicities. These quantities are compared with the experimental ones, which differ from those of ref. [22] due to another selection in space and different sorting variables. Mean energies are also presented and compared with experimental measurements. Error bars for calculation correspond to the two p_0 limits and to the width of corresponding impact parameter bins.

One observes here an overestimation of proton multiplicities in calculation, particularly for the lower impact parameter. The proportion of prompt complex particles decreases when the particle mass increases but increases with the violence of collisions. Multiplicities of deuterons, tritons and ^{3}He seem to be reasonable, if one remembers that contributions of evaporative component and neck emissions are present in experimental data.

For alpha-particles the proportion of calculated prompt emission is quasi-negligible. One could increase the proportion of alpha particles by increasing p_0, but then the calculated spectrum would be too broad, in disagreement with the experiment. On the other hand, the number of prompt ^{4}He can be underestimated, as it can also originate from pre-formed alpha structures in nuclei [2, 55]. Finally it should be remarked that the excess of protons corresponds approximately to the deficit of alphas, multiplied by two. It suggests that the number of cascade protons produced by the ISABEL code is quite correct, and that the calculation is not able to create enough alpha particles.

In refs. [21,22], LCP emission in the mid-velocity region was recognized by an increase of their average transverse energy values. From our simulation it clearly emerges that prompt particle emission is responsible for such a fact. In table 1 we present also mean kinetic energy for various particles. An increase of this value can be observed when the impact parameter decreases. The calculated val-

Table 2. Average total kinetic energy ($E_{\rm kin}$) and total excitation energy ($E^*_{\rm tot}$) obtained from four reaction scenario hypotheses: pure binary reaction scenario (BRS), BRS with prompt emission, pure ternary reaction scenario (TRS), and TRS with prompt emission. The first column refers to different impact parameter windows, the second column gives results of the thrust method applied to obtain QP-QT relative velocity ($v_{\rm rel}$) from the experimental data. Seventh column corresponds to the QP-QT relative velocities, determined with three-sources fits.

b	$v_{\rm rel}$	BRS		BRS + Prompt		$v_{\rm rel}$	TRS		TRS + Prompt	
(fm)	(c)	$E_{\rm kin}$ (MeV)	$E^*_{\rm tot}$ (MeV)	$E_{\rm kin}$ (MeV)	$E^*_{\rm tot}$ (MeV)	(c)	$E_{\rm kin}$ (MeV)	$E^*_{\rm tot}$ (MeV)	$E_{\rm kin}$ (MeV)	$E^*_{\rm tot}$ (MeV)
7-8	0.39	1565	521	1578	459	0.39	1597	397	1720	251
6-7	0.37	1460	625	1497	572	0.39	1404	590	1556	370
5-6	0.34	1225	860	1326	695	0.39	1212	784	1450	516
4-5	0.31	1020	1066	1236	818	0.39	1081	934	1471	399

ues are the *total* kinetic energy of particles, and cannot be directly compared with *transverse* energy values. Nevertheless, as the region selected in momentum space includes only angles between 60 and 120 degrees, the main part of these values is attributed to the transverse motion. Experimental values are evidently smaller than calculated ones (except for protons), which can be attributed to contributions of evaporative components from QP and QT. For protons one observes slightly smaller values for calculation, which are linked with distorted proton energy spectra (see fig. 7). This effect disappears while impact parameter decreases.

4.3 Prompt emission and the total excitation energy of the system

Finally, one can estimate from our calculation the average total excitation energy $E^*_{\rm tot}$ remaining after the prompt emission stage. Note, that one does not presume that $E^*_{\rm tot}$ will be fully thermalized. For estimating $E^*_{\rm tot}$ we take into account two possible hypotheses: binary reaction scenario (BRS) and ternary reaction scenario (TRS). The former corresponds to creation of QP and QT, accompanied possibly by prompt emission. The latter hypothesis concerns creation of an additional neck-like structure in between QP and QT, which can sometimes separate from QP and QT. We shall try to estimate influence of both prompt emission and neck creation effects on $E^*_{\rm tot}$.

General energy balance gives the following formula for $E^*_{\rm tot}$:

$$E^*_{\rm tot} = E_{\rm c.m.} - E_{\rm kin} - Q, \tag{17}$$

where $E_{\rm c.m.}$ is the total kinetic energy available in the center of mass (2085 MeV in our reaction), $E_{\rm kin}$ is the total kinetic energy in the output channel, after prompt emission, but before de-excitation. Q is the mass balance. $E_{\rm kin}$ is given by

$$E_{\rm kin} = E_{\rm rel} + E_{\rm neck} + \sum_i E_i, \tag{18}$$

where $E_{\rm rel}$ is kinetic energy of QP-QT relative motion, $E_{\rm neck}$ is c.m. kinetic energy of the "neck", and $\sum_i E_i$ is the sum of prompt particle energies. Similarly, the mass balance Q splits into

$$Q = M_{\rm QP} + M_{\rm QT} + M_{\rm neck} + \sum_i M_i - (M_{\rm P} + M_{\rm T}), \tag{19}$$

where $M_{\rm QP}$, $M_{\rm QT}$, and $M_{\rm neck}$ are the masses of QP, QT, and "neck" respectively, $\sum_i M_i$ is the sum of prompt particle masses, and $M_{\rm P}$ ($M_{\rm T}$) refers to the mass of projectile (target).

Now, we consider four hypotheses:

1. Pure BRS – with no "neck" and no prompt emission, average masses and charges of QP and QT are assumed to be the same as for projectile and target (average net mass transfer equal to zero).
2. BRS with prompt emission – average masses and charges of QP and QT are given by ISABEL, prompt emission is given by ISABEL + Coalescence calculation in the θ range 0°–180°.
3. Pure TRS with no prompt emission – average QP, QT and "neck" masses are evaluated using three-sources fit measurements [47].
4. TRS with prompt emission – as 3, but the prompt particles obtained in ISABEL + Coalescence model are subtracted from the "neck", and prompt particle kinetic energy is added to the total kinetic energy term.

In the case of binary scenario (1 and 2) the average QP-QT relative velocity is drawn from experimental data using the thrust method [17] (in the current paper all detected particles were used for this analysis). For ternary scenario (3 and 4) the velocities obtained by the three-sources fits [47] were used (the QP-QT relative velocity was found there to be rather constant for all impact parameters, and the "neck" velocity close to mid-rapidity).

The results obtained for four different hypotheses and for four different impact parameter regions are presented in table 2. Comparing the hypotheses "with" and "without" prompt emission one can see, that prompt particle emission decreases $E^*_{\rm tot}$ by about 12–23% in the BRS. This is comparable with influence of "neck" formation (5–24%). In the case of TRS, the amount of excitation energy carried out by prompt emission is about 34–57%, depending on impact parameter. This observation reveals the importance of direct prompt emissions in heavy-ion reactions close to 100 MeV/nucleon.

5 Conclusion

Light charged particles emitted in the intermediate velocity region were studied for the ^{36}Ar + ^{58}Ni reaction at 95 MeV/nucleon. Experimental data have been confronted to result of a calculation performed to predict prompt particle emission. A two step calculation was used. It was composed of the intra-nuclear cascade code ISABEL producing primary prompt protons and neutrons, and of an extended version of the coalescence model producing associated complex particles. This calculation is found to describe rather well proton energy spectra and well the high-energy part of the spectra for emitted light complex particles like deuteron, triton and helium-3. For alpha-particle energy spectra, only the very high energy tail is well reproduced. Thus production of coalescent particles with rather high energies can be found responsible for large transverse energies experimentally observed in the intermediate velocity region at incident energies around 100 MeV/nucleon [21,22].

More quantitatively we can infer from this work that protons emitted in the selected intermediate velocity region come mainly from prompt emission. The proportion of prompt deuterons varies from ∼0.3 to 0.5 when impact parameter decreases. For $A = 3$ particles this proportion reduces to ∼0.1 to 0.3. For alpha-particles the contribution from prompt emission is found very weak revealing the limit of the proposed calculation for heavier particles.

Estimation of total excitation energy of the system shows the importance of prompt emission that was found to carry out about 10–30% of the total excitation energy, depending on the reaction scenario and impact parameter.

Appendix

In the standard version of the model some simplifications were introduced, to obtain an analytical formula for ρ_{ZN}, convenient to determine the p_0 parameter as a fit to experimental data:

1. The integral in eq. (9) is replaced by $V\rho_m(\overrightarrow{p}_c)$; it corresponds to the limit of small p_0 discussed at the beginning of section 2.2.
2. The P_m value in equation (9) is assumed to be independent of m; multiplicity m is replaced by average multiplicity $\overline{m}$, and ρ_m is taken from experiment, *i.e.* it is averaged over all possible multiplicities. This requires also putting $\alpha = 1$ (eq.(15)).
3. A Poisson distribution is assumed for the multiplicity distribution $f(m)$ used in eq. (11):

$$f(m) = \frac{\overline{m}^m}{m!}\exp(-\overline{m}). \tag{A.1}$$

4. The neutron distribution is taken identical to the proton one, corrected for neutron-to-proton ratio in the studied reaction:

$$\rho_n(\overrightarrow{p}) = \frac{N_T + N_P}{Z_T + Z_P}\rho_p(\overrightarrow{p}), \tag{A.2}$$

where ρ_p is the experimentally measured proton distribution.

These assumptions lead to the explicit formula for complex particle density:

$$\rho_{ZN}(\overrightarrow{p}_c) = \left(\frac{N_T + N_P}{Z_T + Z_P}\right)^N \frac{1}{N!Z!}\left(\frac{4}{3}\pi p_0^3\right)^{A-1}[\rho_p(\overrightarrow{p}_c)]^A, \tag{A.3}$$

which corresponds to eq. (2). Let us recall that $\overrightarrow{p}_c$ is a momentum *per nucleon*. For very low incident energies, corrections for Coulomb repulsion have been introduced in [44].

One can remark that inserting $Z = 1$ and $N = 0$ in (A.3) one obtains a correct (*i.e.* observed) proton density. In other words, the formula treats protons (and neutrons) as one-nucleon clusters. Our more precise version of the coalescence model has the same property, but instead of secondary proton density we have to put the primary one.

References

1. D. A. Bromley, *Treatise on Heavy-Ion Science*, (Plenum, New York, 1984).
2. H. Fuchs and K. Möhring, Rep. Prog. Phys. **57**, 231 (1994).
3. H. Nifenecker and J. A. Pinston, Annu. Rev. Nucl. Part. Sci. **40**, 113 (1990).
4. P. Sapienza, R. Coniglione, E. Migneco, C. Agodi, R. Alba, G. Bellia, A. Del Zoppo, P. Finocchiaro, K. Loukachine, C. Maiolino, P. Piattelli, D. Santonocito, Y. Blumenfeld, J. H. Le Faou, T. Suomijarvi, N. Frascaria, J. C. Reyonette, J. A. Scarpaci, J. P. Garron, A. Gillibert, N. Alamanos, F. Auger, A. Péghaire, and Ph. Chomaz, Nucl. Phys. A **630**, 215c (1998).
5. L. Stuttgé, J. C. Adloff, B. Bilwes, R. Bilwes, F. Cosmo, M. Glaser, G. Rudolf, F. Scheibling, R. Bougault, J. Colin, F. Delaunay, A. Genoux-Lubain, D. Horn, C. Lebrun, J. F. Lecolley, M. Louvel, J. C. Steckmeyer, and J. L. Ferrero, Nucl. Phys. A **539**, 511 (1992).
6. B. Lott, S. P. Baldwin, B. M. Szabo, B. M. Quednau, W. U. Schröder, J. Tõke, L. G. Sobotka, J. Barreto, R. J. Charity, L. Gallamore, D. G. Sarantites, D. W. Stracener, and R. T. De Souza, Phys. Rev. Lett. **68**, 3141 (1992).
7. G. Casini, P. G. Bizzeti, P. R. Maurenzig, A. Olmi, A. A. Stefanini, J. P. Wessels, R. J. Charity, R. Freifelder, A. Gobbi, N. Herrmann, K. D. Hildenbrand, and H. Stelzer, Phys. Rev. Lett. **71**, 2567 (1993).
8. F. Bocage, J. Colin, M. Louvel, G. Auger, Ch.O. Bacri, N. Bellaize, B. Borderie, R. Bougault, R. Brou, P. Buchet, J.L. Charvet, A. Chbihi, D. Cussol, R. Dayras, N. De Cesare, A. Demeyer, D. Doré, D. Durand, J.D. Frankland, E. Galichet, E. Genouin-Duhamel, E. Gerlic, D. Guinet, P. Lautesse, J.L. Laville, J.F. Lecolley, R. Legrain, N. Le Neindre, O. Lopez, A.M. Maskay, L. Nalpas, A.D. Nguyen, M. Pârlog, J. Péter, E. Plagnol, M.F. Rivet, E. Rosato, F. Saint-Laurent, S. Salou, J.C. Steckmeyer, M. Stern, G. Tăbăcaru, B. Tamain, O. Tirel, L. Tassan-Got, E. Vient, M. Vigilante, C. Volant, J.P. Wieleczko, C. Le Brun, A. Genoux-Lubain, G. Rudolf , and L. Stuttgé, Nucl. Phys. A **676**, 391 (2000).

9. C. P. Montoya, W. G. Lynch, D. R. Bowman, G. F. Peaslee, N. Carlin, R. T. De Souza, C. K. Gelbke, W. G. Gong, Y. D. Kim, M. A. Lisa, L. Phair, M. B. Tsang, J. B. Webster, C. Williams, N. Colonna, K. Hanold, M. A. McMahan, G. J. Wozniak, and L. G. Moretto, Phys. Rev. Lett. **73**, 3070 (1994).
10. J. F. Lecolley, L. Stuttgé, M. Aboufirassi, B. Bilwes, R. Bougault, R. Brou, F. Cosmo, J. Colin, D. Durand, J. Galin, A. Genoux-Lubain, D. Guerreau, D. Horn, D. Jacquet, J. L. Laville, F. Lefebvres, C. Le Brun, O. Lopez, M. Louvel, M. Mahi, C. Meslin, M. Morjean, A. Péghaire, G. Rudolf, F. Scheibling, J. C. Steckmeyer, B. Tamain, and S. Tomašević, Phys. Lett. B **354**, 202 (1995).
11. J. Tõke, B. Lott, S. P. Baldwin, B. M. Quednau, W. U. Schröder, L. G. Sobotka, J. Barreto, R. J. Charity, L. Gallamore, D. G. Sarantites, D. W. Stracener, and R. T. De Souza, Nucl. Phys. A **583**, 519 (1995); J. Tõke, B. Lott, S. P. Baldwin, B. M. Quednau, W. U. Schröder, L. G. Sobotka, J. Barreto, R. J. Charity, D. G. Sarantites, D. W. Stracener, and R. T. De Souza, Phys. Rev. Lett. **75**, 2920 (1995).
12. M. Colonna, M. Di Toro, A. Guarnera, V. Latora, A. Smerzi, and Z. Jiquan, Nucl. Phys. A **583**, 525 (1995). M. Colonna, M. Di Toro, and A. Guarnera, Nucl. Phys. A **589**, 160 (1995).
13. J. Péter, S. C. Jeong, J. C. Angélique, G. Auger, G. Bizard, R. Brou, A. Buta, C. Cabot, Y. Cassagnou, E. Crema, D. Cussol, D. Durand, Y. El Masri, P. Eudes, Z. Y. He, A. Kerambrun, C Lebrun, R. Legrain, J. P. Patry, A. Péghaire, R. Régimbart, E. Rosato, F. Saint-Laurent, J. C. Steckmeyer, B. Tamain, and E. Vient, Nucl. Phys. A **593**, 95 (1995).
14. A. A. Stefanini, G. Casini, P. R. Maurenzig, A. Olmi, R. J. Charity, R. Freifelder, A. Gobbi, N. Herrmann, K. D. Hildenbrand, M. Petrovici, F. Rami, H. Stelzer, J. P. Wessels, M. Gnirs, D. Pelte, J. Galin, D. Guerreau, U. Jahnke, A. Péghaire, J. C. Adloff, B. Bilwes, R. Bilwes, and G. Rudolf, Z. Phys. A **351**, 167 (1995).
15. J. F. Dempsey, R. J. Charity, L. G. Sobotka, G. J. Kunde, S. Gaff, C. K. Gelbke, T. Glasmacher, M. J. Huang, R. C. Lemmon, W. G. Lynch, L. Manduci, L. Martin, M. B. Tsang, D. K. Agnihotri, B. Djerroud, W. U. Schröder, W. Skulski, J. Tõke, and W. A. Friedman, Phys. Rev. C **54**, 1710 (1996).
16. S. L. Chen, R. T. De Souza, E. Cornell, B. Davin, T. M. Hamilton, D. Hulbert, K. Kwiatkowski, Y. Lou, V. E. Viola, R. G. Korteling, and J. L. Wile, Phys. Rev. C **54**, R2214 (1996).
17. J. Łukasik, J. Benlliure, V. Métivier, E. Plagnol, B. Tamain, G. Auger, Ch. O. Bacri, E. Bisquer, B. Borderie, R. Bougault, R. Brou, Ph. Buchet, J. L. Charvet, A. Chbihi, J. Colin, D. Cussol, R. Dayras, A. Demeyer, D. Doré, D. Durand, P. Eudes, E. Gerlic, D. Gourio, D. Guinet, P. Lautesse, J. L. Laville, J. F. Lecolley, A. Le Fèvre, T. Lefort, R. Legrain, P. Lopez, M. Louvel, N. Marie, L. Nalpas, M. Pârlog, J. Péter, O. Politi, A. Rahmani, T. Reposeur, M. F. Rivet, E. Rosato, F. Saint-Laurent, M. Squalli, J. C. Steckmeyer, M. Stern, L. Tassan-Got, E. Vient, C. Volant, J. P. Wieleczko, M. Colonna, F. Haddad, Ph. Eudes, T. Sami, and F. Sébille, Phys. Rev. C **55**, 1906 (1997).
18. Y. Larochelle, L. Gingras, L. Beaulieu, X. Quian, Z. Saddiki, B. Djerroud, D. Doré, R. Laforest, R. Roy, M. Samri, C. St-Pierre, G. C. Ball, D. R. Bowman, A. Glindo-Uribarri, E. Hagberg, D. Horn, J. A. López, and T. Robinson, Phys. Rev. C **55**, 1869 (1997).
19. P. Pawłowski, J. Brzychczyk, A. J. Cole, P. Désesquelles, W. Gawlikowicz, K. Grotowski, P. Hachaj, S. Micek, R. Płaneta, Z. Sosin, A. Wieloch, D. Benchekroun, E. Bisquer, A. Chabane, A. Demeyer, M. Charvet, B. Cheynis, E. Gerlic, A. Giorni, D. Guinet, D. Heuer, P. Lautesse, L. Lebreton, A. Lléres, M. Stern, L. Vagneron, and J. B. Viano, Phys. Rev. C **57**, 1771 (1998).
20. Y.G. Ma, A. Siwek, J. Péter, F. Gulminelli, R. Dayras, L. Nalpas, B. Tamain, E. Vient, G. Auger, Ch. O. Bacri, J. Benlliure, E. Bisquer, B. Borderie, R. Bougault, R. Brou, J.L. Charvet, A. Chbihi, J. Colin, D. Cussol, E. De Filippo, A. Demeyer, D. Doré, D. Durand, P. Ecomard, P. Eudes, E. Gerlic, D. Gourio, D. Guinet, R. Laforest, P. Lautesse, J. L. Laville, L. Lebreton, J. F. Lecolley, A. Le Fèvre, T. Lefort, R. Legrain, O. Lopez, M. Louvel, J. Łukasik, N. Marie, V. Métivier, A. Ouatizerga, M. Pârlog, E. Plagnol, A. Rahmani, T. Reposeur, M. F. Rivet, E. Rosato, F. Saint-Laurent, M. Squalli, J. C. Steckmeyer, M. Stern, L. Tassan-Got, C. Volant, and J. P. Wieleczko, Phys. Lett. B **390**, 41 (1997).
21. J. C. Angélique, A. Buta, G. Bizard, D. Cussol, A. Péghaire, J. Péter, R. Popescu, G. Auger, R. Brou, C. Cabot, E. Crema, Y. El Masri, P. Eudes, Z. Y. He, A. Kerambrun, C. Lebrun, R. Regimbart, E. Rosato, F. Saint-Laurent, J. C. Steckmeyer, B. Tamain, and E. Vient, Nucl. Phys. A **614**, 261 (1997).
22. T. Lefort, D. Doré, D. Cussol, Y. G. Ma, J. Péter, R. Dayras, M. Assenard, G. Auger, Ch. O. Bacri, F. Bocage, R. Bougault, R. Brou, Ph. Buchet, J. L. Charvet, A. Chbihi, J. Colin, A. Demeyer, D. Durand, P. Eudes, J. D. Frankland, E. Galichet, E. Genouin-Duhamel, E. Gerlic, M. Germain, D. Gourio, D. Guinet, B. Hurst, P. Lautesse, J. L. Laville, J. F. Lecolley, A. Le Fèvre, R. Legrain, N. Le Neindre, O. Lopez, M. Louvel, A.M. Maskay, L. Nalpas, A.D. N'Guyen, M. Pârlog, E. Plagnol, G. Politi, A. Rahmani, T. Reposeur, E. Rosato, F. Saint-Laurent, S. Salou, J. C. Steckmeyer, M. Stern, F. Saint-Laurent, S. Salou, J.C. Steckmeyer, M. Stern, G. Tăbăcaru, B. Tamain, L. Tassan-Got, O. Tirel, E. Vient, C. Volant, J. P. Wieleczko, and A. Wieloch, Nucl. Phys. A **662**, 397 (2000)
23. A. Bonasera, F. Gulminelli, and J. Molitoris, Phys. Rep. **243**, 1 (1994).
24. J. Aichelin and G. F. Bertsch, Phys. Rev. C **31**, 1730 (1985).
25. C. Grégoire, B. Remaud, F. Sébille, L. Vinet, and Y. Raffray, Nucl. Phys. A **465**, 317 (1987).
26. Ph. Eudes, Z Basrak, and F. Sébille, Phys. Rev. C **56**, 2003 (1997).
27. P. Danielewicz and G. F. Bertsch, Nucl. Phys. A **533**, 712 (1991).
28. M. Beyer, C. Kuhrts, G. Röpke and P. D. Danielewicz, nucl-th/9910058/ (1999).
29. P. Danielewicz, and Q. Pan, Phys. Rev. C **46**, 2002 (1992).
30. D. Prindle, A. Elmaani, C. Hide-Wright, W. Jiang, A. A. Sonzogni, R. Vandenbosch, D. Bowman, G. Cron, P. Danielewicz, J. Dinius, W. Hsi, W. G. Lynch, C. Montoya, G. Peaslee, C. Schwartz, M. B. Tsang, C. Williams, R. T. De Souza, D. Fox, and T. Moore, Phys. Rev. C **57**, 1305 (1998).

31. A. Ono, *Proceedings of 7-th International Conference on "Clustering Aspects of Nuclear Structure and Dynamics", Rab, Croatia*, (World Scientific, 1999) page 284.
32. Y. Yariv and Z. Fraenkel, Phys. Rev. C **20**, 2227 (1979); Phys. Rev. C **24**, 488 (1981).
33. K. Chen, Z.Fraenkel, G. Friedlander, J. R. Grover, J. M. Miller, and Y. Shimamoto, Phys. Rev. **166**, 942 (1968).
34. C. Donzaud, Ph.D. thesis, IPN Orsay, IPNO-T-93-05 (1993).
35. S. T. Butler and C. A. Pearson, Phys. Rev. **129**, 836 (1963).
36. H. H. Gutbrod, A. Sandoval, P. J. Johansen, A. M. Poskanzer, J. Gosset, W. G. Meyer, G. D. Westfall, and R. Stock, Phys. Rev. Lett. **37**, 667 (1976).
37. J. Gosset, H. H. Gutbrod, W. G. Meyer, A. M. Poskanzer, A. Sandoval, R. Stock, and G. D. Westfall, Phys. Rev. C **16**, 629 (1977).
38. M. C. Lemaire, S. Nagamiya, S.Schnetzer, H.Steiner, and I. Tanihata, Phys. Lett. B **85**, 38 (1979).
39. S. Nagamiya, M. C. Lemaire, E. Moeller, S. Schnetzer, G. Shapiro, H. Steiner, and I. Tanihata, Phys. Rev. C **24**, 971 (1981).
40. R. L. Auble, J. B. Ball, F. E. Bertrand, C. B. Fulmer, D. C. Hensley, I. Y. Lee, R. L. Robinson, P. H. Stelson, and C. Y. Wong, Phys. Rev. C **28**, 1552 (1983).
41. J. L. Nagle, B. S. Kumar, D. Kusnezov, H.Sorge, and R. Mattiello, Phys. Rev. C **53**, 367 (1996).
42. A. Schwarzschild and C. Zupančič, Phys. Rev. **129**, 854 (1963).
43. A. Mekjian, Phys. Rev. Lett. **38**, 640 (1977); Phys. Rev. C **17**, 1051 (1978).
44. T. C. Awes, G. Poggi, C. K. Gelbke, B. B. Back, B. G. Glagola, H. Breuer, and V. E. Viola Jr, Phys. Rev. C **24**, 89 (1981).
45. J. Pouthas, B. Borderie, R. Dayras, E. Plagnol, M.F. Rivet, F. Saint-Laurent, J.C. Steckmeyer, G. Auger, C.O. Bacri, S. Barbey, A. Barbier, A. Benkirane, J. Benlliure, B. Berthier, E. Bougamont, P. Bourgault, P. Box, R. Bzyl, B. Cahan, Y. Cassagnou, D. Charlet, J.L. Charvet, A. Chbihi, T. Clerc, N. Copinet, D. Cussol, M. Engrand, J.M. Gautier, Y. Huguet, O. Jouniaux, J.L. Laville, P. Le Botlan, A. Leconte, R. Legrain, P.Lelong, M. Le Guay, L. Martina, C. Mazur, P. Mosrin, L. Olivier, J. P. Passerieux, S. Pierre, B. Piquet, E. Plaige, E.C. Pollacco, B. Raine, A. Richard, J. Ropert, C. Spitaels, L. Stab, D. Sznajderman, L. Tassan-Got, J. Tiller, M. Tripon, P. Vallerand, C. Volant, P. Volkov, J.P. Wieleczko, and G. Wittwer, Nucl. Instrum. Meth. A **357**, 418 (1995).
46. G. Tăbăcaru, B. Borderie, A. Ouatizerga, M. Pârlog, M.F. Rivet, G. Auger, Ch.O. Bacri, F. Bocage, R. Bougault, R. Brou, Ph. Buchet, J.L. Charvet, A. Chbihi, J. Colin, D. Cussol, R. Dayras, A. Demeyer, D. Doré, D. Durand, P. Ecomard, J.D. Frankland, E. Galichet, E. Genouin-Duhamel, E. Gerlicf, D. Guinet, P. Lautesse, J.L. Laville, A. Le Fèvre, T. Lefort, R. Legrain, N. Le Neindre, O. Lopez, M. Louvel, L. Nalpas, A.D. Nguyen, E. Plagnol, E. Rosato, F. Saint-Laurent, S. Salou, M. Squalli, J.C. Steckmeyer, M. Stern, L. Tassan-Got, O. Tirel, E. Vient, C. Volant, and J.P. Wieleczko, Nucl. Instrum. Meth. A **428**, 379 (1999).
47. D. Doré, Ph. Buchet, J.L. Charvet, R. Dayras, L. Nalpas, D. Cussol, T. Lefort, R. Legrain, C. Volant, G. Auger, Ch.O. Bacri, N. Bellaize, F. Bocage, R. Bougault, B. Bouriquet, R. Brou, A. Chbihi, J. Colin, A. Demeyer, D. Durand, J.D. Frankland, E. Galichet, E. Genouin-Duhamel, E. Gerlic, D. Guinet, S. Hudan, P. Lautesse, F. Lavaud, J.L. Laville, J.F. Lecolley, C. Leduc, N. Le Neindre, O. Lopez, M. Louvel, A.M. Maskay, J. Normand, M. Pârlog, P. Pawłowski, E. Plagnol, M.F. Rivet, E. Rosato, F. Saint-Laurent, J.C. Steckmeyer, M. Stern, G. Tăbăcaru, B. Tamain, L. Tassan-Got, O. Tirel, E. Vient, and J.P. Wieleczko, Phys. Lett. B **491**, 15 (2000).
48. B. Borderie, F. Gulminelli, M.F. Rivet, L. Tassan-Got, M. Assenard, G. Auger, F. Bocage, R. Bougault, R. Brou, Ph. Buchet, J. Colin, R. Dayras, A. Demeyer, J.D. Frankland, E. Galichet, E. Genouin-Duhamel, E. Gerlic, M. Germain, D. Guinet, P. Lautesse, J.L. Laville, J.F. Lecolley, T. Lefort, R. Legrain, N. Le Neindre, M. Louvel, A.M. Maskay, L. Nalpas, A.D. Nguyen, M. Pârlog, E. Plagnol, A. Rahmani, T. Reposeur, E. Rosato, F. Saint-Laurent, S. Salou, J.C. Steckmeyer, M. Stern, G. Tăbăcaru, B. Tamain, O. Tirel, D. Vintache, and C. Volant, Eur. Phys. J. A **6**, 197 (1999).
49. J-F. Lecolley, E. Galichet, D. Guinet, R. Bougault, F. Gulminelli. G. Auger, Ch-O. Bacri, F. Bocage, B. Borderie, R. Brou, P. Buchet, J-L. Charvet, A. Chbihi, J. Colin, D. Cussol, R. Dayras, A. Demeyer, D. Doré, D. Durand, J.D. Frankland, E. Genouin-Duhamel, E. Gerlic, P. Lautesse, J-L. Laville, T. Lefort, R. Legrain, N. Le Neindre, O. Lopez, M. Louvel, A-M. Maskay, L. Nalpas, A.D. Nguyen, M. Pârlog, J. Péter, E. Plagnol, M-F.Rivet, E. Rosato, F. Saint-Laurent, J-C. Steckmeyer, M. Stern, G. Tăbăcaru, B. Tamain, L. Tassan-Got, O. Tirel, E. Vient, C. Volant, and J-P. Wieleczko, Nucl. Instr. and Meth. A **441**, 517 (2000).
50. J. Péter, D. Cussol, G. Bizard, R. Brou, M. Louvel, J. P. Patry, R. Regimbart, J. C. Steckmeyer, J. P. Sullivan, B. Tamain, E. Crema, H. Doubre, K. Hagel, G. M. Jin, A. Péghaire, F. Saint-Laurent, Y. Cassagnou, R. Legrain, C. Lebrun, E. Rosato, R. Mac Grath, S. G. Jeong, S. M. Lee, Y. Nagashima, T. Nakagawa, M. Ogihara, J. Kasagi, and T. Motobayashi, Nucl. Phys. A **519**, 611 (1990).
51. H. Ströbele, R. Brockmann, J. W. Harris, F. Reiss, A. Sandoval, R. Stock, K. L. Wolf, H. G. Pugh, L. S. Schroeder, R. E. Renfort, K. Tittel, and M. Maier, Phys. Rev. C **27**, 1349 (1983).
52. J. F. Lecolley, D. Durand, M. Aboufirassi, R. Bougault, J. Colin, A. Genoux-Lubain, C. Lebrun, O. Lopez, M. Louvel, C. Meslin, G. Rudolf, L. Stuttgé, and S. Tomašević, Phys. Lett. B **387**, 460 (1996).
53. P. Pawłowski, D. Benchekroun, E. Bisquer, J. Brzychczyk, A. Chabane, M. Charvet, B. Cheynis, A. J. Cole, A. Demeyer, P. Désesquelles, W. Gawlikowicz, E. Gerlic, A. Giorni, K. Grotowski, D. Guinet, P. Hachaj, D. Heuer, P. Lautesse, L. Lebreton, A. Lléres, S. Micek, R. Płaneta, Z. Sosin, M. Stern, L. Vagneron, J. B. Viano, and A. Wieloch, Z. Phys. A **357**, 387 (1997).
54. C. Cavata, M. Demoulins, J. Gosset, M. C. Lemaire, D. D. L'Hôte, J. Poitou, and O. Valette, Phys. Rev. C **42**, 1760 (1990).
55. T. Neff, H. Feldmeier, R. Roth, and J. Schnack, *Proceedings of the XXVII International Workshop on Gross Properties of Nuclei and Nuclear Excitations, Hirschegg, Austria*, edited by H. Feldmeier, J. Knoll, W. Nörenberg and J. Wambach, (GSI, 1999) p. 283.